

SYNTHESIS OF PURE AND MANGANESE DOPED ZINC OXIDE NANOPARTICLES BY A SOLUTION GROWTH TECHNIQUE: STRUCTURAL AND OPTICAL INVESTIGATION

Raymond A. Antwi, Isaac Nkrumah*, Francis K. Ampong, Mark Paal, Reuben Y. Tamakloe, Robert K. Nkum, Francis Boakye

Department of Physics, Kwame Nkrumah University of Science and Technology, Kumasi, Ghana

**Corresponding Author email: inkrumah.sci@knust.edu.gh*

Received August 8, 2023; revised September 22, 2023; accepted September 25, 2023

Pure and manganese doped zinc oxide nanoparticles have been successfully synthesized over the composition range, $Zn_{1-x}Mn_xO$ ($0 < x < 0.5$), by a solution growth process. The effect of Mn doping on the structure, morphology and optical properties were investigated by several techniques. X-Ray diffraction studies confirmed the formation of a single-phase polycrystalline hexagonal wurtzite structure of ZnO within the range, $0 < x < 0.3$. No Mn related secondary phases were detected, within this range, which could be attributed to the fact that the dopant atoms had been well incorporated into the ZnO crystal lattice. For $Zn_{1-x}Mn_xO$ ($x = 0.5$), several low intensity peaks belonging to remnants of Manganese acetate were observed in the diffractogram, establishing a solubility limit for the synthesis technique used. The variation of d-spacing with Mn percent doping showed a very good agreement with Vergard's law within the range ($0 < x < 0.25$). EDAX analysis of the nanoparticles was consistent with the formation of Mn doped ZnO. The optical band gap of the ZnO nanoparticles decreased linearly with increasing Mn percent doping, suggesting the possibility of tuning the band gap of ZnO by doping with Mn.

Keywords: *Manganese doped zinc oxide; Solution phase process; Crystal structure; Optical band gap*

PACS: 81.15.Fg, 61.05.C, 42.70.Qs

INTRODUCTION

Metal oxides display a wide range of properties which have useful technological applications, and the possibility of varying these properties by various techniques, has resulted in these compounds being widely studied. Most of the interesting properties displayed by these metal oxides are obtained by doping with transition metals such as; Fe, Co, Ni, Mn and Cu.

Among several metal oxides, ZnO is attracting attention due to its efficiency, low cost, non-toxic nature, and being chemically and mechanically stable [1]. In addition, the relatively large band gap of ZnO (3.37 eV) coupled with its high exciton binding energy (60 meV) at room temperature, renders it a superb host material for doping with Transition metals [2]. Manganese has a peculiar nature, it has several oxidation states, causing diverse chemical and structural forms [3], [4]. These properties make it an important dopant for binary compounds. An additional advantage is the ease of Mn incorporation into the ZnO lattice, due to the relatively small difference in ionic radii between Mn^{2+} and Zn^{2+} [5]. An efficient dopant must not cause any structural change when it is incorporated in the host atom [6]. These and many other technological as well as potential applications have been well documented in literature.

With the renewed interest in the properties of these nanomaterials, there is the need to transition towards synthesis techniques which are environmentally friendly, simple, and less costly. Available literature suggests that within the past decade several publications have emerged on the synthesis of pure and Mn-doped ZnO.

Techniques which have generated a lot of interest are the solution growth methods. These techniques usually involve the use of simple, inexpensive equipment, and can be carried out at low temperatures. An additional advantage, the ability to control the size of the ZnO nanostructures [7].

Controlling metastable phases, particle sizes and morphologies are also some of the benefits provided by the low temperature chemical route for synthesizing nanomaterials [8]. In spite of the advantages offered by this technique, incorporation of Mn in ZnO lattice by this route is challenging because of the higher bond energy of Mn-O compared to Zn-O, this means more energy would be needed to substitute Zn^{2+} with Mn^{2+} in ZnO lattice. A process which is easily attainable with high temperature techniques [9].

The solubility limit, which is the extent to which the Mn dopant can be incorporated in the ZnO lattice without causing any structural defects, is another important feature worth taking into account. Beyond this doping limit, the structure degrades due to the presence of secondary phases formed by Mn clusters that do not replace Zn^{2+} in ZnO lattice [10-12].

In our previous work, Armah et al. [13], we reported on the solubility of Mn in ZnO Nanocrystallites grown by wet chemical synthesis. Pure ZnO was obtained at a synthesis temperature of 200 °C. Below this temperature, the diffractogram showed several impurity peaks/secondary phases. For the $Zn_{1-x}Mn_xO$ nanocrystallites, synthesized at 200 °C the solubility limit was < 20 % and for a synthesis temperature of 180°C, it was < 0.5 %. Beyond these limits, peaks indexed to secondary phases were observed in the diffractogram.

To adopt this technique in producing high-quality pure and Mn doped ZnO nanoparticles, with desirable qualities, for device applications, requires an improvement on the solubility limit. In this current paper, we present a more effective low-temperature route to synthesize $Zn_{1-x}Mn_xO$ nanoparticles by a solution phase process. The method used is a modification of the solution growth process reported in our previous work. In comparison with other solution phase processes which use synthesis temperatures above 200 °C, this work uses a relatively lower temperature of about 110°C. No sophisticated equipment is used and no toxic gases are released during this process. The resulting changes in the structural, morphology and optical properties of the nanoparticles are examined.

MATERIALS AND METHODS

The precursors used were zinc acetate dihydrate ($Zn(CH_3COO)_2 \cdot 2H_2O$) and anhydrous manganese acetate ($Mn(CH_3COO)_2$), methanol (CH_3OH), absolute ethanol (C_2H_5OH) and 2 M ammonium hydroxide (NH_4OH), all obtained from Merck limited, India.

Synthesis of Pure ZnO Nanocrystals

In the synthesis procedure, 50 g of zinc acetate was ground in an agate mortar into a fine powder. The zinc acetate powder was poured into a beaker. 150 ml of methanol was added to the zinc acetate to dissolve it. The beaker and its content were sonicated for 40 minutes until all the solute was dissolved. Dropwise addition of 2 M ammonium hydroxide solution was added to the mixture to obtain a pH of 8. The solution mixture was kept for about 3 hours before it was placed on a hot plate and heated slowly in incremental steps of 10 °C (each temperature held for 15 minutes) until a final temperature of 64 °C was reached for complete dissolution of precursors. At this temperature all the excess water content evaporated and the solution turned into a gel-like material. The temperature was increased further and the resultant gel-like material was maintained at 110 °C until it solidified into pale yellow crystals. These were then allowed to cool down to ambient conditions and ground into fine particles. They were then washed thrice with water, once with ethanol and dried at 100 °C overnight. Afterwards the samples were calcined at 500 °C for 3 hours to produce the ZnO Nanocrystals

The preference for metal acetate precursors, Methanol, etc. have been well explained [13, 14]. The ammonium hydroxide, supplied the oxide oxygen whilst the acetate acts as base. It should be mentioned that, apart from the synthesis temperature which differs, other post synthesis processes such as washing the nanoparticles in water and ethanol, drying overnight at 100 °C, and calcining were not done in our previous work.

Synthesis of $Zn_{1-x}Mn_xO$

Specific amounts of the metallic precursors were ground into a fine powder. The same procedure for the synthesis of ZnO described above was used. The solution appeared creamy at low dopant concentrations and became pinkish as the concentration increased. The same procedure was carried out for $Zn_{1-x}Mn_xO$ ($0 < x < 0.5$).

RESULTS AND DISCUSSION

Powder X-Ray Diffraction Analysis

The crystal structure of the nanoparticles was studied by a PANalytical Empyrean Series 2 powder X-ray diffractometer in the 2θ range 5 to 99 °C with $CuK\alpha$ (1.5406 Å) radiation.

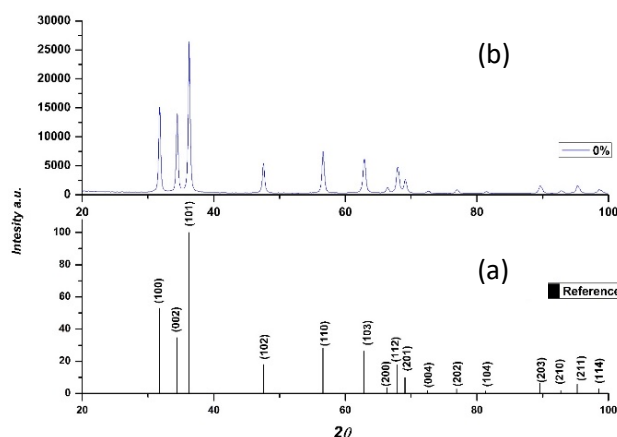


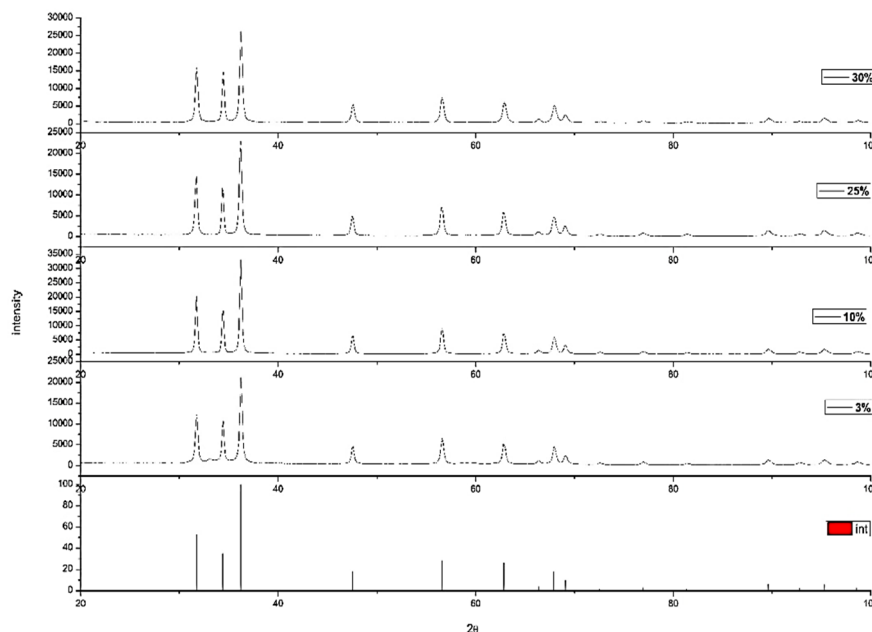
Figure 1. (a) Stick pattern for the hexagonal wurtzite structure of ZnO (Ref. Code 01-079-9897) (b) XRD pattern of pure ZnO

Figure 1a and 1b show the stick pattern for the hexagonal wurtzite structure of ZnO (Ref. Code 01-079-9897) and the XRD pattern for pure ZnO nanoparticles respectively. It can be observed that the pattern of prominent peaks in Figure 1(b), are indexed to the hexagonal wurtzite structure of ZnO, the peak corresponding to the (101) plane being the most intense. Authors from other studies have reported similar observations. The lack of any impurity peaks in the diffractogram affirms the purity of the ZnO nanoparticles. Table 1 shows the pattern list which confirms the composition and purity of the synthesized ZnO nanoparticles.

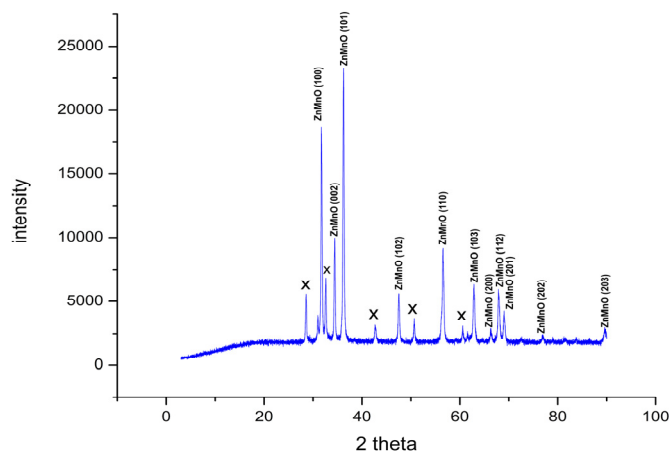
Table 1. Pattern List of the synthesized ZnO nanoparticles.

Visible	Ref.Code	Score	Compound Name	Displ.[°2 θ]	Scale Fac.	Chem. Formula
*	01-079-9878	99	Zinc Oxide	0.000	1.032	Zn O

It is worth noting that most reports on the production of ZnO by wet chemical synthesis, such as Armah et al. [15] achieved this level of purity only after synthesizing at temperatures above 180 °C.

**Figure 2a.** XRD patterns of $Zn_{1-x}Mn_xO$ ($0 < x < 0.5$) nanoparticles

The X-Ray diffraction patterns of $Zn_{1-x}Mn_xO$ ($0 < x < 0.5$) nanoparticles are shown in Figure 2a. The well-defined peaks in all the samples are indexed to pure hexagonal wurtzite structured ZnO with preferred orientation along the (101) plane. Similar observations have been reported by Guermat et al. [16].

**Figure 2b.** XRD pattern for $Zn_{1-x}Mn_xO$ ($x = 0.5$)

The sharpness of the peaks in the diffractogram indicates good crystallinity. We can also see that no secondary phases are observed as compared to our previous work. In the occurrence where there are no discernable peaks indexed to Mn related secondary phases, one may safely conclude that the Mn is replacing Zn^{2+} in the ZnO lattice. This view is buttressed by Shatnawi et al. [17]. It is also worth noting that whilst some authors; Sebayang et al. [18] have reported a similar behavior with regard to the most intense peak, others such as Singh et al. [19], reported the (002) planes as being the most intense peak. There was a slight shift in 2 theta position with Mn doping percentage.

The XRD pattern of Figure 2b shows that apart from the prominent peaks indexed to the ZnO hexagonal structure, there are several low intensity peaks (labelled as x) which do not belong to any of the phases of $Zn_{1-x}Mn_xO$. These impurities are remnants of Manganese acetate in the sample. Thus, based on the synthesis technique used in this work, the doping limit for $Zn_{1-x}Mn_xO$ can be estimated to be in between $0.3 < x < 0.5$. This is an improvement on our previous study using wet chemical synthesis which resulted in the appearance of secondary phases of Mn_2O_3 at $x = 0.2$ [13]. Table 2 gives a summary of some parameters obtained from the peak analysis.

Table 2. Peak shifting of the (101) plane with Mn doping percentage

% of Mn doping	2Theta position of (101) plane	FWHM	d-spacing[Å]
0	36.2637	0.3100	2.47727
3	36.2506	0.3100	2.47813
10	36.2315	0.4133	2.47940
25	36.2080	0.3100	2.48095
30	36.2497	0.4133	2.47819
50	36.2020	0.4133	2.47930

Observations from Table 2 indicate that, with the exception of the sample with 30 % Mn doping, there is a slight shift in 2-Theta position of the (101) plane, towards lower values, with increasing Mn doping percentage and a corresponding increase in the d-spacing. As mentioned in the introductory chapters, Mn can exist in different oxidation states, such as Mn²⁺, Mn³⁺ Mn⁴⁺ etc. Thus, when Mn substitutes for Zn²⁺ the lattice has to expand or contract depending on which of the oxidation states of Mn is present. The exact distribution of Mn in the lattice cannot be easily ascertained [20] [21]. If Mn²⁺ ion which has a much larger ionic radius replaces Zn²⁺, the peaks will shift towards the lower 2-theta angles due to an increase in d-spacing [13]. Thus, the observed shift in d-spacing with Mn doping percentage shown in Table 2, can be associated with the higher ionic radius of Mn²⁺.

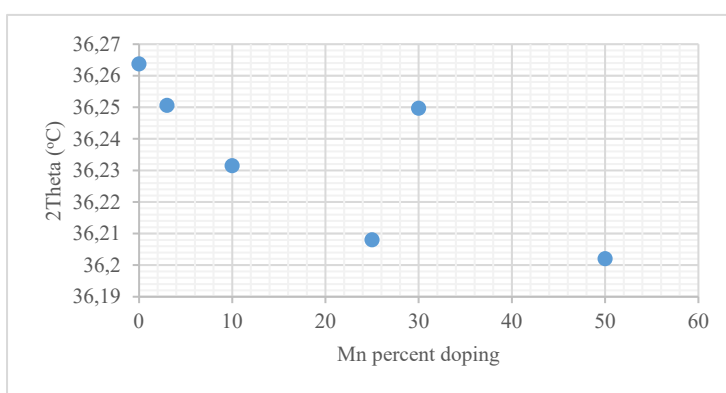


Figure 3. Plot of peak shifting of the (101) plane with Mn doping percentage

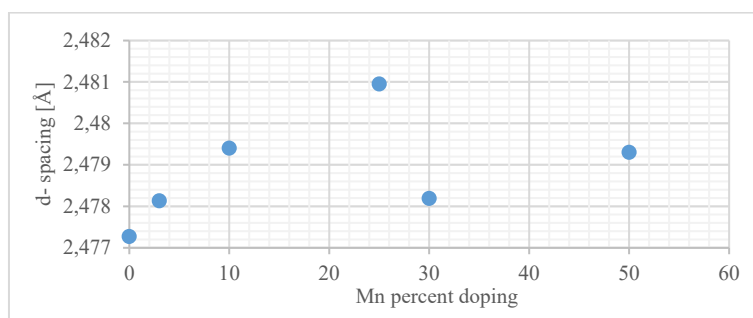


Figure 4. Variation of the d-spacing of the (101) plane with Mn doping percentage

Figure 3 shows the shift in 2Theta position of the (101) plane with Mn percent doping, whilst Figure 4 shows the corresponding increase in d-spacing.

There is a linear dependence of the lattice parameters of mixed crystals with composition, and this is true for substituted solid solutions [22]. This linear dependence, referred to as Vegard's law is consistent with the likely behavior of an ideal mixed phase [23]. It is also worth noting that, although there are some publications which hold contrary views to the validity of this law [24], other authors such as Muralikrishna et al. [25] are of the view that Vegard's law is mostly valid in a narrow compositional range. The later view is supported by observations made in Figure 4: variations of the d-spacing with Mn doping percentage is linear up to about 25 % Mn doping. Beyond this range the variation is non-linear.

Average grain size

The average grain size was calculated using the formula given by Scherrer [26], [27]:

$$D = \frac{K\lambda}{\beta \cos \theta}$$

Where K is a constant, the X-ray wavelength $\lambda = 1.541 \text{ \AA}$, β is the full width at half maximum of the most intense peak, which is the (101) plane, θ is the Bragg angle of the (hkl) planes associated to the structure. The average grain size, D for the entire samples, Zn_{1-x}Mn_xO (0 < x < 0.50), was about 28 nm.

SEM and EDAX Analysis

SEM and EDX analyses were carried out using a Zeiss SmartEDX Instrument (15 kV nominal electron beam voltage). Figures 5, 6, and 7 show the SEM and EDAX results of pure ZnO and some Mn doped ZnO.

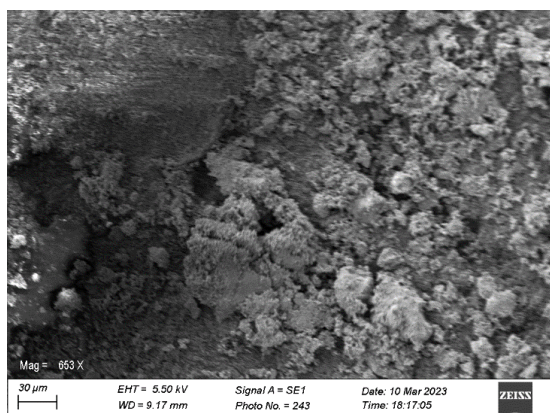


Figure 5a. SEM Micrograph of pure ZnO

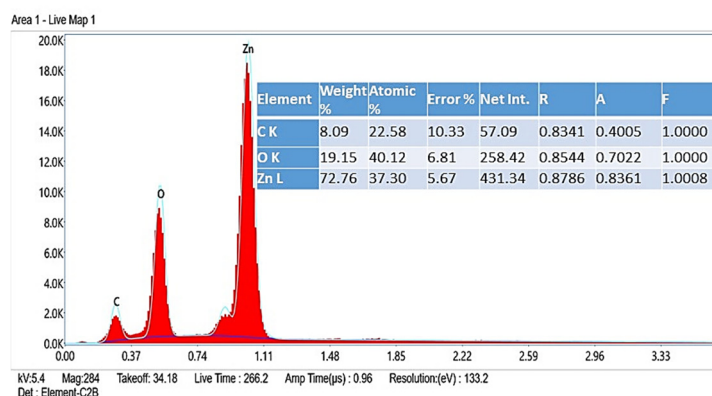


Figure 5b. EDAX Spectrum of pure ZnO

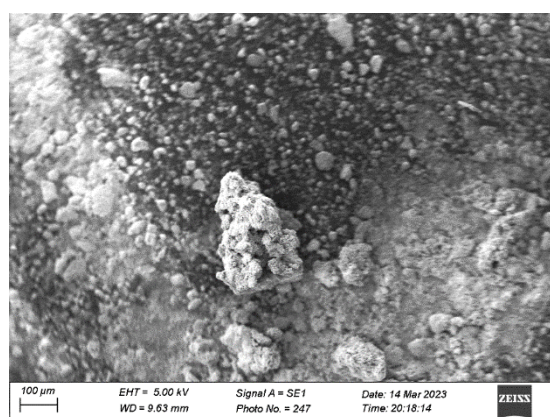


Figure 6a. SEM Micrograph of Mn doped ZnO (10 % Mn doping)

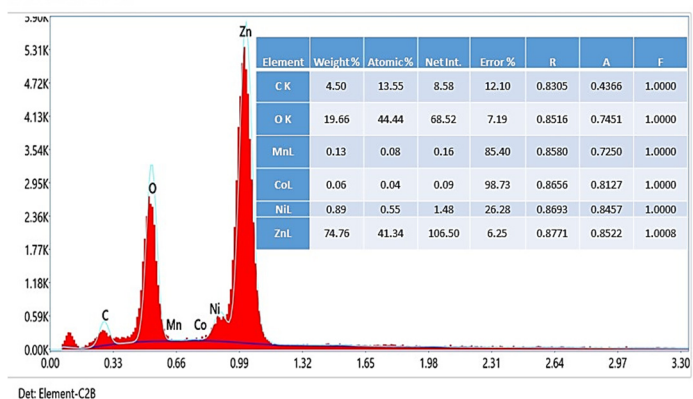


Figure 6b. EDAX Spectrum of Mn doped ZnO (10 % Mn doping)

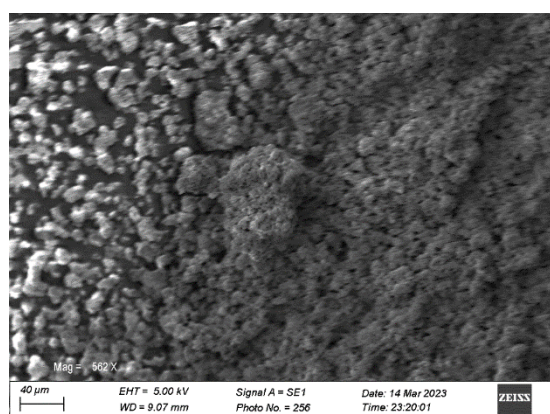


Figure 7a. SEM Micrograph of Mn doped ZnO (50 % Mn doping)



Figure 7b. EDAX Spectrum of Mn doped ZnO (50 % Mn doping)

The EDAX spectrum in Figure 5b, indicates that the synthesized nanoparticle is pure ZnO. A close observation of the EDAX spectra of Figures 6b and 7b clearly confirm that the synthesized nanoparticles contain zinc (Zn), oxygen (O), and manganese (Mn). Other elements seen in the tables of Figures 6b and 7b may emanate from the SEM specimen stub used a substrate in the analysis. All the SEM images show the occurrence of clusters.

Optical Analyses

The absorbance spectra of the $Zn_{1-x}Mn_xO$ ($0 < x < 0.5$) nanoparticles, dispersed in potassium hydroxide (KOH, 7.5 M), were obtained using a ANALYTIK JENA - SPECORD 200 PLUS- 223E1451 UV-VIS spectrophotometer.

Figure 8 shows the optical absorption spectra for the $Zn_{1-x}Mn_xO$ ($0 < x < 0.50$) nanoparticles. Generally, there was an increase in absorbance with Mn incorporation. The absorption edge shifted towards the higher wavelengths with increasing Mn doping. This red shift suggests an increase in size of the Mn-doped ZnO. A similar situation was reported by Thakur et al. [28].

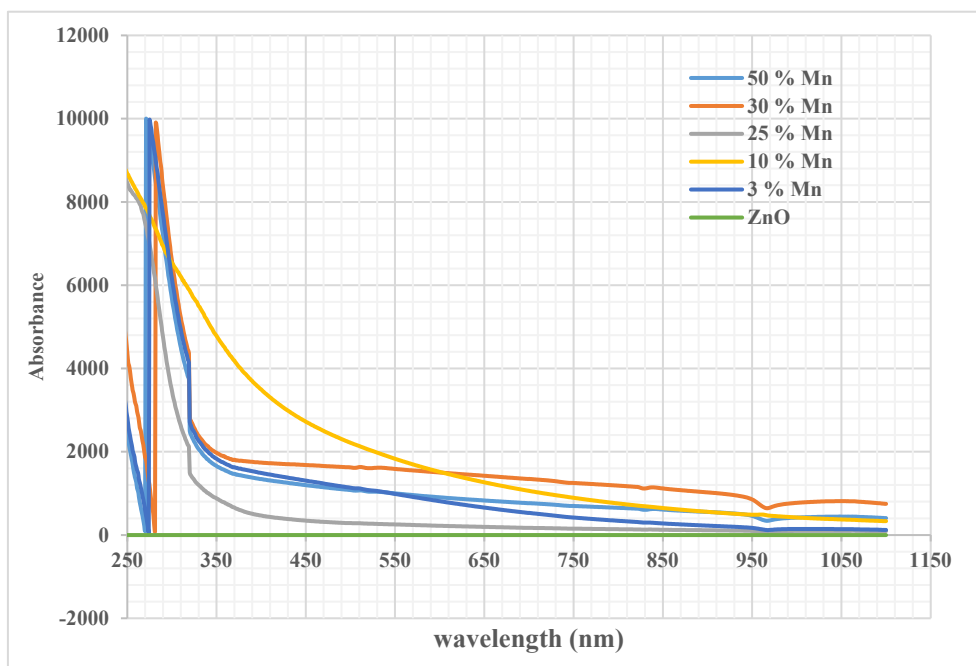


Figure 8. Optical absorption spectra for the $Zn_{1-x}Mn_xO$ ($0 < x < 0.50$) nanoparticles

Determination of the optical band gap

The band gap and type of transition were determined by the Stern equation [29].

$$(Ah\nu) = [K(h\nu - E_g)]^n$$

where A is the absorbance, $h\nu$ is the photon energy, n takes on the value of $1/2$ or 2 depending on whether the optical transitions are indirect or indirect [30], and K is a constant. The band gap E_g is determined by first plotting a graph of $(Ah\nu)^{1/n}$ vs $h\nu$. ZnO is a direct band gap material so $n = 1/2$, the band gap, E_g is obtained from the intercept on the $h\nu$ axis. A plot of $(Ah\nu)^2$ vs $h\nu$ for ZnO, 10 and 25 % Mn doped ZnO are shown Figure 9, 10 and 11 respectively.

From Figure 9, the estimated band gap for ZnO is 3.30 eV.

From Table 3, it can be observed that there is a general decrease in the band gap of the nanoparticles with increasing Mn percentage doping. Abdel-Galil et al. [30] have given reasons for the observed decrease in band gap. A plot of the variation in estimated band gaps with Mn percentage doping is shown in Figure 12.

The linear nature of the graph in Figure 12, suggests the possibility of tuning the band gap of ZnO by doping with Mn. The red shift observed in the absorption maxima due to doping with Mn, is ascribed to the decrease in the energy band gap, which makes it favorable for photocatalytic applications [28].

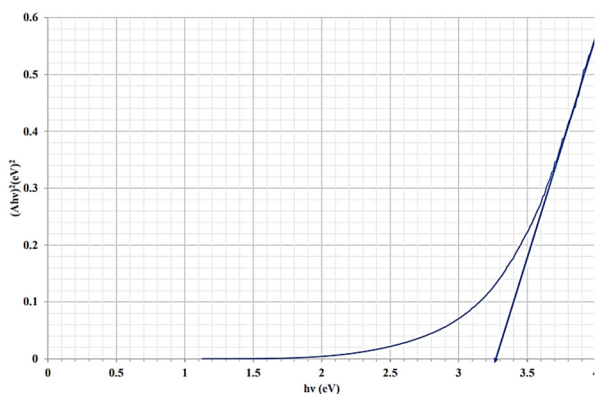


Figure 9. A plot of $(Ah\nu)^2$ vs $h\nu$ for ZnO

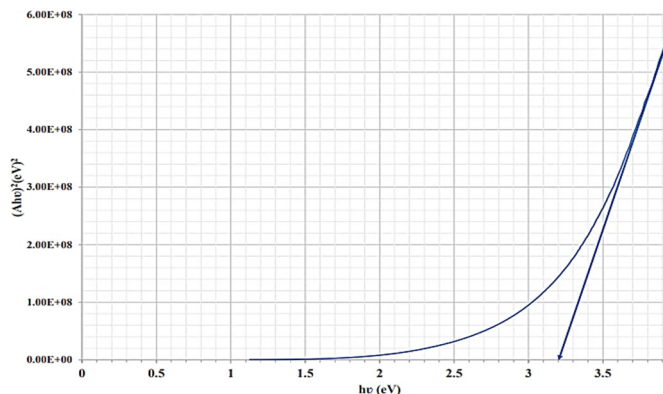


Figure 10. A plot of $(Ah\nu)^2$ vs $h\nu$ for 10 % Mn doping

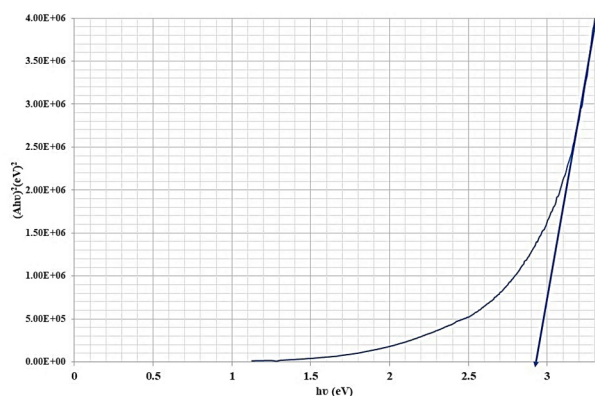


Figure 11. A plot of $(Ahv)^2$ vs hv for 25 % Mn doping

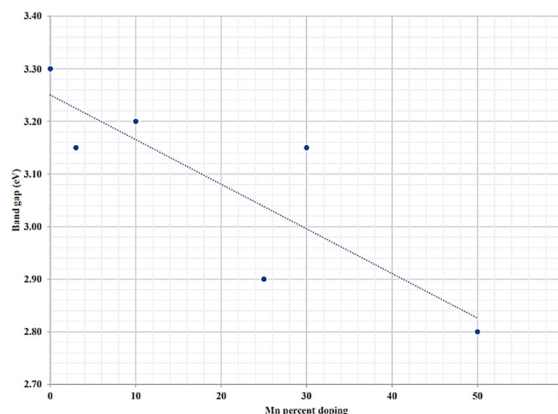


Figure 12. Plot of estimated band gaps against Mn percent doping

Table 3. Summary of the estimated band gaps for $Zn_{1-x}Mn_xO$ ($0 < x < 0.50$) nanoparticles

Mn percent doping (%)	Estimated band gap (eV)
0	3.30
3	3.15
10	3.20
25	2.90
30	3.15
50	2.80

CONCLUSIONS

Nanoparticles of $Zn_{1-x}Mn_xO$ ($0 < x < 0.5$) have been successfully synthesized by a low-temperature solution growth method. All the detectable peaks in the diffractogram were indexed as ZnO with hexagonal wurtzite structure. For the doping range of $0 < x < 0.3$, no additional peaks were observed in the diffractogram confirming the formation of pure and single phase of $Zn_{1-x}Mn_xO$ within this range of Mn doping. For $Zn_{1-x}Mn_xO$ ($x = 0.5$), several low intensity peaks belonging to remnants of Manganese acetate were observed in the diffractogram. Thus, in this work, the solubility limit for $Zn_{1-x}Mn_xO$ can be estimated to be in between $0.3 < x < 0.5$. This is an improvement on our previous study using wet chemical synthesis which resulted in the appearance of secondary phases of Mn_2O_3 at $x = 0.2$. The variation in d-spacing with Mn doping percentage was linear within the range ($0 < x < 0.25$) suggesting the formation of a substitutional solid solution. EDAX confirmed the presence of Mn. The optical band gap of the nanoparticles decreased with increasing Mn percent doping. Overall, it is possible to synthesize good quality manganese doped zinc oxide nanoparticles, especially in the zinc rich end of the composition by adopting the synthesis technique used in this work.

ORCID

- © Isaac Nkrumah, <https://orcid.org/0000-0003-4030-7931>; © Francis K. Ampong, <https://orcid.org/0000-0003-3562-8183>
 © Mark Paal, <https://orcid.org/0000-0002-6465-2708>; © Reuben Y. Tamakloe, <https://orcid.org/0000-0002-5563-5930>
 © Robert K. Nkum, <https://orcid.org/0000-0003-0404-760X>; © Raymond A. Antwi, <https://orcid.org/0000-0002-3488-7143>

REFERENCES

- [1] P. Chaudhary, F. Fatima, and A. Kumar, *Journal of inorganic and organometallic polymers and materials*, **30**, 5180 (2020). <https://doi.org/10.1007/s10904-020-01674-8>
- [2] R.N. Ali, H. Naz, J. Li, X. Zhu, P. Liu, and B. Xiang, *Journal of Alloys and Compounds*, **744**, 90 (2018). <https://doi.org/10.1016/j.jallcom.2018.02.072>
- [3] F. Giovannelli, A.N. Ndimba, P. Diaz-Chao, M. Motelica-Heino, P.I. Raynal, C. Autret, and F. Delorme, *Powder Technology*, **262**, 203 (2014). <https://doi.org/10.1016/j.powtec.2014.04.065>
- [4] M. Gotić, T. Jurkin, S. Musić, K. Unfried, U. Sydlik, and A. Bauer-Šegvić, *Journal of Molecular Structure*, **1044**, 248 (2013). <https://doi.org/10.1016/j.molstruc.2012.09.083>
- [5] G. Voicu, O. Oprea, B. S. Vasile, and E. Andronescu, *Journal of Nanomaterials and Biostructures*, **8**(2), 667 (2013). https://chalcogen.ro/667_Voicu.pdf
- [6] R. Buonsanti, and D.J. Milliron, *Chemistry of Materials*, **25**(8), 1305 (2013). <https://doi.org/10.1021/cm304104m>
- [7] A.K. Singh, G.S. Thool, P.R. Bangal, S.S. Madhavendra, and S.P. Singh, *Industrial & Engineering Chemistry Research*, **53**(22), 9383 (2014). <https://doi.org/10.1021/ie500077v>
- [8] N. Singh, S. Mittal, K.N. Sood, and P.K. Gupta, *Chalcogenide Letters*, **7**(4), 275 (2010). http://chalcogen.ro/275_Singh.pdf
- [9] D. Wu, Z. Huang, G. Yin, Y. Yao, X. Liao, D. Han, X. Huang, and J. Gu, *Cryst. Eng. Comm.* **12**(1), 192 (2010). <https://doi.org/10.1039/B909780E>
- [10] A.S. Hassan, K. Abdalla, and A.M. Moanes, *IJSRSET*, **3**(8), 94 (2017). <https://ijsrset.com/paper/3167.pdf>
- [11] T.M. Dhruvashi, and P.K. Shishodia, *Adv. Mater. Lett.*, **7**(2), 116 (2016). <https://doi.org/10.5185/amlett.2016.5966>
- [12] A. Boumezoued, K. Guergouri, M. Zaabat, D. Recham, and R. Barille, in: *Proceedings of International Agricultural, Biological & Life Science Conference*, edited by Y. Kaya, and T. Popova, (Edirne, Turkey, 2018), 250-258.

- [13] E.N.A. Armah, F.K. Ampong, M. Egblewogbe, H.A. Koffi, F. Boakye, J.K.A. Amuzu, and R.K. Nkum, *Advanced Nano Research*, **2**(1), 53 (2019). <https://doi.org/10.21467/anr.2.1.53-61>
- [14] T.J. Jacobsson, *Naturvetarprogrammet Kemi*, (Uppsala Universitet, 2009).
- [15] E.N.A.A. Armah, M. Egblewogbe, H.A. Koffi, A.A. Yankson, F.K. Ampong, F. Boakye, J.K.A. Amuzu, and R.K. Nkum, *Adv. Nan. Res.* **3**(1), 28 (2020). <https://doi.org/10.21467/anr.3.1.28-39>
- [16] N. Guermat, W. Daranfedi, I. Bouchama, and N. Bouarissa, *Journal of Molecular Structure*, **1225**, 129134 (2021). <https://doi.org/10.1016/j.molstruc.2020.129134>
- [17] M. Shatnawi, A.M. Alsmadi, I. Bsoul, B. Salameh, M. Mathai, G. Alnawashi, G.M. Alzoubi, et al., *Results in Physics*, **6**, 1064(2016). <https://doi.org/10.1016/j.rinp.2016.11.041>
- [18] P. Sebayang, C. Kurniawan, R.Y. Lubis, I. Priyadi, and D. Aryanto, *Makara Journal of Science*, **24**(2), 5 (2020). <https://doi.org/10.7454/mss.v24i1.11914>
- [19] A.K. Singh, G.S. Thool, P.R. Bangal, S.S. Madhavendra, and S.P. Singh, *Industrial & Engineering Chemistry Research*, **53**(22), 9383 (2014). <https://doi.org/10.1021/ie500077v>
- [20] R. Saravanan, F. Santhanam, and J.L. Berchmans, *Chemical Papers*, **66**(3), 226 (2012). <https://doi.org/10.2478/s11696-011-0129-8>
- [21] D.S. Cook, J.E. Hooper, D.M. Dawson, J.M. Fisher, D. Thompsett, S.E. Ashbrook, and R.I. Walton, *Inorganic Chemistry*, **59**(6), 3805 (2020). <https://doi.org/10.1021/acs.inorgchem.9b03459>
- [22] U. Hotjie, C. Rose, and M. Binnewies, *Solid State Sciences*, **5**(9), 1259 (2003). [https://doi.org/10.1016/S1293-2558\(03\)00177-8](https://doi.org/10.1016/S1293-2558(03)00177-8)
- [23] F.K. Ampong, J.A.M. Awudza, R.K. Nkum, F. Boakye, P.J. Thomas, and P. O'Brien, *Solid State Sciences*, **40**, 50 (2015). <https://doi.org/10.1016/j.solidstatedsciences.2014.12.013>
- [24] B. Clavier, A. Zhadan, T. Baptiste, F. Boucher, A. Guet, F. Porcher, V. Brezová, et al., *Dalton Transactions*, **51**(21), 8411 (2022). <https://doi.org/10.1039/D2DT00352J>
- [25] G.M. Muralikrishna, B. Tas, N. Esakkiraja, V.A. Esin, K.H. Kumar, I.S. Golovin, I.V. Belova, et al., *Acta Materialia*, **203**, 116446 (2021). <https://doi.org/10.1016/j.actamat.2020.10.065>
- [26] E.A. Botchway, F.K. Ampong, I. Nkrumah, D.B. Puzer, R.K. Nkum, and F. Boakye, *East European Journal of Physics*, **2**, 249 (2023). <https://doi.org/10.26565/2312-4334-2023-2-28>
- [27] M. Paal, I. Nkrumah, F.K. Ampong, D.U. Ngbiche, R.K. Nkum, and F. Boakye, *Science Journal of University of Zakho*, **8**(3), 97 (2020). <https://doi.org/10.25271/sjuoz.2020.8.3.752>
- [28] D. Thakur, A. Sharma, A. Awasthi, D.S. Rana, D. Singh, S. Pandey, and S. Thakur, *Chemosensors*, **8**(4), 120 (2020). <https://doi.org/10.3390/chemosensors8040120>
- [29] I. Nkrumah, F.K. Ampong, A. Britwum, M. Paal, B. Kwakye-Awuah, R.K. Nkum, and F. Boakye, *Chalcogenide Letters*, **20**(3), 205 (2023). <https://doi.org/10.15251/CL.2023.203.205>
- [30] A. Abdel-Galil, M.R. Balboul, and A. Sharaf, *Physica B*, **477**, 20 (2015). <https://doi.org/10.1016/j.physb.2015.08.001>

СИНТЕЗ ЧИСТИХ ТА ЛЕГОВАНИХ МАРГАНЦЕМ НАНОЧАСТИНОК ОКСИДУ ЦИНКУ З РОЗЧИНУ: СТРУКТУРНО-ОПТИЧНЕ ДОСЛІДЖЕННЯ

Реймонд А. Антві, Ісаак Нкрума, Френсіс К. Ампонг, Марк Паал, Рубен Й. Тамакло, Роберт К. Нкум, Френсіс Боак'є
Факультет фізики, Університет науки і технологій Кваме Нкрума, Кумасі, Гана

Чисті та леговані марганцем наночастинки оксиду цинку були успішно синтезовані в діапазоні складу $Zn_{1-x}Mn_xO$ ($0 < x < 0,5$) за допомогою процесу росту з розчину. Вплив легування Mn на структуру, морфологію та оптичні властивості досліджували кількома методами. Рентгеноструктурні дослідження підтвердили формування однофазної полікристалічної гексагональної структури вюрциту ZnO в діапазоні $0 < x < 0,3$. Жодних вторинних фаз, пов'язаних з Mn, у цьому діапазоні не виявлено, що можна пояснити тим фактом, що атоми легуючої домішки були добре включені в кристалічну решітку ZnO. Для $Zn_{1-x}Mn_xO$ ($x = 0,5$) на дифрактограмі спостерігалось кілька піків низької інтенсивності, що належать до залишків ацетату марганцю, що встановлює межу розчинності для використаної методики синтезу. Зміна d-інтервалу з процентним легуванням Mn показала дуже хорошу узгодженість із законом Вергарда в діапазоні ($0 < x < 0,25$). Аналіз наночастинок EDAX підтвердив утворення ZnO, легovanого Mn. Оптична заборонена зона наночастинок ZnO зменшувалася лінійно зі збільшенням відсотка легування Mn, що свідчить про можливість налаштування ширини забороненої зони ZnO шляхом легування Mn.

Ключові слова: оксид цинку легований марганцем; фази процесу розчину; кристалічна структура; оптична заборонена зона